J. Fluid Mech. (1981), *vol.* 112, *pp.* 225–251
Printed in Great Britain

An investigation of internal solitary waves in a two-fluid system

By C. GARY KOOP AND GERALD BUTLER
Fluid Mechanics Department, TRW/DSSG, One Space Park,
Redondo Beach, California 90278

(Received 1 August 1980)

The results of an experimental investigation dealing with finite-amplitude internal solitary waves in a two-fluid system are presented. Particular attention is paid to characterizing solitons in terms of their shape and amplitude–wavelength scale relationship. Two cases are considered, *viz.*, a shallow- and a deep-water configuration, in order to study the depth effect upon the propagational characteristics of the waves. Comparisons are made between the experimental results and existing internal-wave theories. In addition, discussion is presented describing how these existing theories may be extended to include higher-order nonlinear and viscous effects.

1. Introduction

The study of finite-amplitude effects in internal-wave systems has received a great deal of attention in recent years from numerous investigators; notably Benney (1966), Benjamin (1966, 1967), Davis & Acrivos (1967), Ono (1975), Kubota, Ko & Dobbs (1977), among others. The recent observations of large-scale solitary wave motions in both the atmosphere (Christy, Muirhead & Hales 1978) and in the ocean (Osborn & Burch 1980; Osborne, Burch & Scarlet 1978) have generated additional interest in this phenomenon.† Much of the theoretical work which has been done has been concerned with analysing fluid motion in systems where the internal waves are weakly nonlinear and are in some sense long relative to the overall depth of the fluid. Following what is, by now, a familiar procedure, one may describe these wave motions by balancing nonlinear and dispersive effects in the governing equations. Such a procedure leads directly to an expression governing the long-time evolution of the stream function, which is the Korteweg–de Vries equation. This equation has been studied a great deal within the past decade and methods have been established to construct exact analytical solutions for arbitrarily prescribed initial conditions (cf. Segur 1973).

In addition to these shallow-water theories, effort has been spent in analysing nonlinear internal wave motion in fluids of infinite extent (Benjamin 1967; Ono 1975). Here, long waves are measured relative to an internal length scale characteristic of the thermocline region, rather than the total fluid depth. For this infinite-depth problem, dispersion enters at lower order, and the resulting stream-function evolution equation has a dispersive term which is a Hilbert transform. This contrasts with the triple-derivative term found in the Korteweg–de Vries equation. Recently, Kubota

† An interesting account of the practical difficulties associated with oil-drilling activities in the presence of 100 m internal solitary waves is presented in *Oil and Gas Journal*, 17 September, 1979, pp. 66–67.

et al. (1978) derived an evolution equation which interpolates between these shallow- and deep-water limits. This equation, which is valid provided the thermocline thickness is sufficiently smaller than the total fluid depth, has a dispersive term that is a transcendental integral operator, and which reduces to a triple derivative and a Hilbert transform in the shallow- and deep-water limits, respectively.

In contrast to the great deal of analytical work which has been done, there appears to be a dearth of experimental study dealing with finite-amplitude effects on long internal waves. Walker (1973), in an investigation of internal interfacial waves in a two-fluid system, presents data over a limited range of depth ratios, but these results are somewhat inconclusive due to the dominance of viscous effects and the small tank size used. Yates (1978) recently made measurements of nonlinear wave motions in a continuously stratified system. However, a majority of these experiments were made at fairly large wave amplitudes, and no definite conclusion could be drawn regarding the accuracy of any of the aforementioned weakly nonlinear theories. More recently, Kao & Pao (1979) presented experimental measurements of solitary-wave propagation for a thin pycnocline stratification. These results, however, were confined to shallow-water conditions and no attempt was made to establish whether the spatial scales of the waves, correlated with some measure of the wave amplitude, were consistent with the shallow-water theory.

The primary motivation for the present investigation is to try and fill this experimental void and provide a quantitatively reliable data base, upon which one may assess the validity and determine the regions of applicability of the various theories dealing with finite-amplitude internal waves. Our particular concern will be to study how the important characteristics of these waves are altered, owing to the changing importance of the dispersive terms, as one proceeds from a shallow-water system to one which is in some sense deep. In pursuing this problem, it is felt that the most convenient experimental approach is to consider pulse-like permanent waveform disturbances whose characteristics can be readily compared with the analytic solitary-wave solutions of the relevant evolution equations. In these comparisons between the theories and the experiments, special emphasis will be placed upon some of the geometrical features of the disturbances, such as profile shape, and the functional relationship between the amplitude of a solitary wave and its wavelength. As will be discussed, we feel that this amplitude–wavelength scaling represents the most fundamental difference between the various theories, and experimentally is the most definitive way of establishing the domain of validity of each theory. A less sensitive criterion would involve the use of phase speed measurements, but as will be shown such measurements would have to be extremely precise in order for the data to be useful in discriminating between theories.

In addition to the aforementioned discussion, a secondary intent of this investigation is to discuss how some of the existing internal-wave theories may be extended to include higher-order nonlinear effects or viscous effects, and to indicate when these corrections are important.

2. Theoretical description

2.1. *Review of existing theoretical analyses*

All of the existing analytical work relevant to the nonlinear internal-wave studies conducted in the present investigation may be roughly categorized as follows:
(*a*) shallow-water theory (Benjamin 1966)

$$\lambda/H \gg 1, \quad h/H = O(1);$$

(*b*) deep-water theory (Benjamin 1967; Ono 1975)

$$\lambda/H \to 0, \quad \lambda/h \gg 1;$$

(*c*) finite-depth theory (Kubota *et al.* 1978)

$$\lambda/h \gg 1, \quad h/H \ll 1;$$

where λ is a measure of the horizontal extent of the wave, h is an intrinsic length scale associated with the density stratification (e.g. the thermocline thickness) and H is the total fluid depth.

All of these theories may (at least to first order) be cast in the framework of a generalized evolution equation commonly known as Whitham's equation which is written as

$$\frac{\partial \eta}{\partial t} + c_1 \eta \eta_x + \frac{\partial}{\partial x} \int_{-\infty}^{\infty} \eta(x', t)\, dx' \frac{1}{2\pi} \int_{-\infty}^{\infty} c(k)\, e^{ik(x-x')} dk = 0. \tag{1}$$

Here, $\eta(x, t)$ measures the internal wave displacement field, $c(k)$ is the linear dispersion law (with c_0 being the linear long-wave phase speed), and c_1 is a functional of the $k = 0$ eigenfunction.

For shallow-water internal waves, Benjamin (1966) shows that the linear dispersion law expanded for small wavenumbers k has the quadratic dependence

$$\frac{c(k) - c_0}{c_0} \sim k^2,$$

and, for this case, Whitham's equation reduces to the familiar Korteweg–de Vries (KdV) equation

$$\frac{\partial \eta}{\partial t} + c_0 \eta_x + c_1 \eta \eta_x + c_2 \eta_{xxx} = 0.$$

(The actual definitions of c_0, c_1 and c_2 may be found in the cited reference and are not repeated here.) The solitary-wave solution to this equation has been known for some time and is given by

$$\eta(x - ct) = a\, \mathrm{sech}^2 \frac{x - ct}{\lambda}, \tag{3a}$$

where

$$c = c_0 + \frac{ac_1}{3}, \quad a\lambda^2 = 12 \frac{c_2}{c_1}. \tag{3b, c}$$

Here, a is the maximum displacement and c is the phase speed correct to $O(a/H)$. From equation (3*c*) one observes that the solitary-wave amplitude–wavelength scaling required for a wave to be described correctly by the shallow-water theory is

$$\lambda/H = O(a/H)^{-\frac{1}{2}}. \tag{3d}$$

Benjamin (1967) and Ono (1975) consider the problem of an infinite-depth fluid, where the internal wave is long relative to the intrinsic length scale h, associated with the density stratification. Waves in this system are more dispersive than shallow-water waves, the expanded dispersion law having linear rather than quadratic dependence upon k, and the resulting evolution equation (often called the Benjamin–Ono equation) is written

$$\frac{\partial \eta}{\partial t} + c_0 \eta_x + c_1 \eta \eta_x + c_2 H(\eta_{xx}) = 0, \tag{4}$$

where $H(\eta_{xx})$ denotes the Hilbert transform of η_{xx}.

The solitary-wave solution to this equation has been found by Benjamin (1967) to be the Lorentzian profile given by

$$\eta(x-ct) = \frac{a\lambda^2}{(x-ct)^2+\lambda^2}, \tag{5a}$$

where

$$c = c_0 + \tfrac{1}{4} a c_1, \tag{5b}$$

$$a\lambda = -4c_2/c_1. \tag{5c}$$

It is of interest to note that the character of the solitary-wave amplitude–wavelength scaling required for this deep-water system, *viz.*

$$\lambda/h = O(a/h)^{-1}, \tag{5d}$$

is distinct from the shallow-water scaling given by equation (3*d*). Much of the subsequent discussion regarding the experimental results will focus upon this distinction. We remark here that, in our opinion, this amplitude–wavelength scaling is the most fundamental difference between the shallow- and deep-water theories, and represents the most sensitive way of establishing the domain of validity for each theory. For parameters typical of this experimental investigation, wavelength predictions of the two theories may differ by more than 100 % for a given wave amplitude. Thus, high experimental accuracy is not a requirement for discrimination between the theories. Furthermore, regression statistics (particularly on log–log plots) utilizing the entire data base may be used to establish whether the KdV scaling $\lambda/h \sim \epsilon^{-\frac{1}{2}}$ or the Benjamin–Ono scaling $\lambda/h \sim \epsilon^{-1}$ (where $\epsilon \equiv a/h$) is most appropriate for a given system. Of lesser concern, we feel, is the degree to which the two theories are able to predict the experimentally measured phase speeds. This is because both theories predict a linear dependence of phase speed upon wave amplitude. Thus, to discriminate between the two predictions one must be able to resolve *slight* differences in the slopes of the amplitude–phase-speed relationship. We emphasize that these differences are small. For parameters typical of our experiment, phase-speed measurements would have to be made to an accuracy of about 1 % before differences between the two theories could be resolved. As a consequence, we have chosen to use the amplitude–wavelength scale relationship as the primary basis for our assessments.

In addition to the KdV and Benjamin–Ono theories, Kubota *et al.* (1977) derived an evolution equation governing the propagation of long waves in fluids which are neither shallow nor deep, and in which the thermocline is much smaller than the total

fluid depth. In this case, the dispersion law has the transcendental wavenumber dependence

$$\frac{c(k)-c_0}{c_0} \sim k \coth kh,$$

and the finite-depth evolution equation resulting from this dispersion law is given by

$$\frac{\partial \eta}{\partial t}+c_0\eta_x+c_1\eta\eta_x+c_2\frac{\partial^2}{\partial x^2}\int_{-\infty}^{\infty}\eta(x',t)\left[\coth\frac{\pi}{2H}(x-x')-\operatorname{sgn}\frac{(x-x')}{H}\right]dx'. \tag{6}$$

Kubota *et al.* note that the finite-depth equation reduces to the KdV and Benjamin–Ono equations in the shallow- and deep-water limits, respectively.

The solitary-wave solution to this equation has been found by Joseph (1977) to be

$$\eta(x-ct) = a\Big/\left(\cosh^2\frac{x-ct}{\lambda}+\left[\tan\frac{H}{\lambda}\sinh\frac{x-ct}{\lambda}\right]^2\right), \tag{7a}$$

where

$$c = c_0-2c_2\left[1-\frac{2H}{\lambda}\cot\frac{2H}{\lambda}\right], \tag{7b}$$

$$a\lambda\cot\frac{H}{\lambda} = -\frac{8c_2}{c_1}. \tag{7c}$$

As can be seen from equation (7*c*), the solitary-wave amplitude–wavelength scaling in a finite-depth system is transcendental, which contrasts with the algebraic relationships derived in the KdV and Benjamin–Ono analyses.

It is worth noting at this point that all of the previously described evolution equations possess soliton as well as solitary-wave solutions, as demonstrated by Segur (1973) (KdV), Meiss & Pereira (1978), Chen, Lee & Pereira (1979) (Benjamin–Ono) and Kubota *et al.* (1978) (finite depth).

All of the analyses which have been discussed up to this point are first-order theories, so that terms of order (a/h) have been retained in the analysis but the second-order nonlinear and dispersive terms are neglected. However, the experimental data (to be discussed) involve waves having amplitudes as large as $a/h \approx 0{\cdot}6$. For these disturbances the assumption of weak nonlinearity might no longer be valid. To assess what effect the inclusion of higher-order terms has upon the solitary-wave amplitude–wavelength scaling, we have extended the KdV analysis for a two-fluid internal wave system to $O(a/h)^2$ (details of the derivation and definition of the various constants are presented in appendix A). The resulting evolution equation takes the form

$$\frac{\partial \eta}{\partial t}+c_0\eta_x+c_1\eta\eta_x+c_2\eta_{xxx}+c_3\eta_{5x}+c_4(\eta\eta_{xx})_x+c_5(\eta^3)_x+c_6(\eta_x^2)_x = 0. \tag{8}$$

The solitary-wave solution to this extended evolution equation is given by

$$\eta(x,t) = a\operatorname{sech}^2\frac{x-ct}{\lambda}\left[1+\frac{a}{h}C\tanh^2\frac{x-ct}{\lambda}\right]+O\left[\left(\frac{a}{h}\right)^3\right]. \tag{9a}$$

The solitary-wave amplitude–wavelength relationship is given by

$$\left(\frac{h}{\lambda}\right)^2 = \alpha^{(1)}\frac{a}{h}+\alpha^{(2)}\left(\frac{a}{h}\right)^2, \tag{9b}$$

and (for later reference)

$$\lambda_I = (\alpha^{(1)}a/h)^{-\frac{1}{2}}\left\{1 - a\left[2\alpha^{(1)}h\left(\alpha^{(2)} - \frac{2}{3}\alpha^{(1)}C\right)\right]^{-1}\right\}, \tag{9c}$$

where $\alpha^{(1)}$, $\alpha^{(2)}$ and C are defined in appendix A. We remark here that the analysis presented in appendix A considers both the rigid lid and free surface boundary conditions. For conditions typical of the present experimental configuration, however, the quantitative differences between the two analyses is not large. For example, in the shallow-water configuration (discussed in the next section), at $\lambda/h = 10$ the second-order rigid-lid theory yields $a/h = 0{\cdot}0676$, whereas in the free-surface analysis $a/h = 0{\cdot}0579$. For comparison, the first-order results are $a/h = 0{\cdot}0577$ (rigid lid) and $a/h = 0{\cdot}0552$ (free surface). For consistency with the finite-depth theory (which incorporates the rigid-lid boundary condition), all of the subsequent KdV calculations will be based upon the rigid-lid analysis.

2.2. *Viscous effects*

Preliminary experiments, which are described in §3, revealed that in the present facility the influence of viscosity upon the internal-wave propagation characteristics could not be neglected. It was observed, for example, that, for conditions typical of a majority of the experiments, viscous stresses produce a 50 per cent attenuation in the internal-wave amplitude as the disturbance propagates one length of the tank. Clearly, the previously discussed inviscid theories are incapable of describing such phenomena, and this provided the motivation for a theoretical effort designed to study analytically the effect viscosity has upon the experimentally generated internal waves.

One simple model which proves to be useful is Keulegan's (1948) analysis for the gradual viscous damping of surface gravity waves. This model has been modified to include internal interfacial waves in a two-fluid system. In essence, the theory assumes that the energy dissipation in the viscous boundary layers along the solid surfaces and within the interface region is balanced by a net decrease in the solitary-wave amplitude. The compensation for this amplitude attenuation is an increase in horizontal extent of the wave such that the fundamental KdV scale relationship $\lambda/H = \alpha\epsilon^{-\frac{1}{2}}$ is preserved. Details of the analysis are presented in appendix B. The resulting expression governing the solitary-wave amplitude decay is given by

$$\frac{\epsilon(x)}{\epsilon_0} = \left[1 + K\epsilon_0^{\frac{1}{4}}\frac{x - x_0}{h_1}\right]^{-4}, \tag{10a}$$

where

$$K = \frac{1}{2\pi^{\frac{3}{2}}}\frac{\nu_1^{\frac{1}{2}}c^{\frac{3}{2}}}{\alpha^{\frac{1}{4}}h_1^{\frac{3}{2}}g(\rho_1 - \rho_2)/\rho_1}\left[2\left(1 + \frac{h_1}{B}\right) + \left(\frac{h_1}{h_2}\right)^2\frac{\rho_2}{\rho_1}\left(\frac{\nu_2}{\nu_1}\right)^{\frac{1}{2}}\left(1 + \frac{2h_2}{B}\right)\right]. \tag{10b}$$

(One may refer to appendix B for definition of the various parameters appearing in the above expressions.) These equations reduce to the expressions derived by Keulegan (1948) (with one small proviso as noted in appendix B) in the limit $\rho_2 \to 0$.

The preceding expressions present a convenient way of calculating wave amplitude attenuation, providing the initial disturbance is a solitary wave and one is considering a two-fluid system. It is also of interest, however, to describe the evolution of internal waves emanating from arbitrary initial conditions and propagating through a viscous medium having a variable density gradient. A related problem, *viz.* the evolution

equation for a shallow-water surface gravity wave in a viscous fluid, has been derived by Kakutani & Matsuuchi (1975) and solved numerically by Matsuuchi (1976). This analysis has been extended here to include internal-wave systems. The details of the analysis are presented in appendix C. The resulting equation governing the evolution of the stream function

$$\psi(x,z,t) = f(\xi,\tau)\,\phi(z)$$

is given by

$$f_\tau + c_1 f f_\xi + c_2 f_{\xi\xi\xi} = c_3 \int_\xi^\infty \frac{\partial f}{\partial \xi'} \frac{d\xi'}{(\xi'-\xi)^{\frac{1}{2}}}, \tag{11}$$

where c_1 and c_2 are the same coefficients defined for the inviscid KdV equation and

$$c_3 = \frac{\frac{1}{2}\left(\frac{g}{H}\right)^{\frac{1}{4}}\left(\frac{c_0}{\pi}\right)^{\frac{1}{2}}\left[\frac{\bar{\rho}(H)\,\phi'^2(H)}{R_2^{*\frac{1}{2}}} + \frac{\bar{\rho}(0)\,\phi'^2(0)}{R_1^{*\frac{1}{2}}}\right]}{\int_0^H \bar{\rho}(\phi')^2\,dz}. \tag{12}$$

(The various quantities are defined in appendix C.) Although no exact solution to the above equation has been identified analytically, solutions have been obtained numerically using the pseudo-spectral technique of Fornberg (1977). Presentation of the results of these calculations, however, is deferred until after discussion of some of the experimental results.

3. Experimental results and comparison with theory

3.1. *Experimental apparatus and procedure*

The experiments were performed in the TRW internal-wave facility which is shown schematically in figure 1. The wave tank, constructed from $\frac{1}{2}$ in Plexiglas, is approximately 6 metres long and has a 45 cm × 60 cm cross-section. The lower boundary of the tank consists of a specially constructed false bottom, fabricated with reinforced blancher ground tooling plate, which was introduced in order to minimize variations in bottom topography. Over the 6 metre length of the channel, the average variation in bottom elevation is less than about $\pm 0{\cdot}02$ cm. Note that there is no wave-absorption device at the downstream end of the tank, so that waves are free to reflect off the end wall and propagate back through the test section.

The fluid system chosen for use in experimentation consists of two mutually immiscible liquids having different specific gravities. Several considerations went into the choice of this system. First of all, the two-layer stratification is an extremely simple system, and it is believed that there is no advantage in using a system which is, in some sense, more complicated (e.g. continuous salt stratification). All of the physics relevant to the present study, *viz.* nonlinearity, dispersion, ability to vary overall fluid depth, existence of an intrinsic internal length scale, etc., are contained in the simple two-fluid system. Secondly, the two-fluid system is particularly well suited for providing quantitatively reliable experimental data, because the interface is always well defined and experiments are quite repeatable. As a by-product of having an interface which is, for all practical purposes, infinitesimally thin, wave-amplitude measurements may be made in a straightforward and unambiguous manner

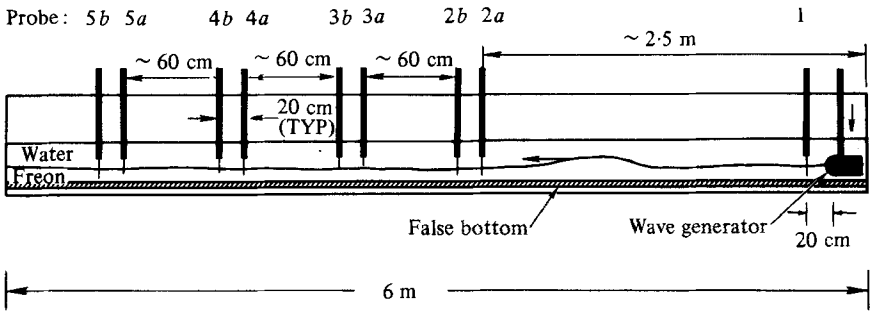

FIGURE 1. Schematic diagram of experimental apparatus.

using capacitance gauges, and since each displacement measurement requires the use of only a single probe (in contrast to the probe arrays required in continuously stratified fluids) one is free to use several such probes longitudinally displaced in order to study the spatial evolution of a disturbance.

The immiscible fluids chosen for use in this investigation were Freon TF (specific gravity 1·58, $\nu = 0{\cdot}0044$ cm^2 s^{-1}) and deionized water. To keep the fluid system as clean as possible, both the water and the Freon were filtered using 5 μm filters prior to being introduced into the tank. In addition, a surface skimmer was utilized in order to ensure that the interface between these two fluids remained clean during the experiments.

Interfacial disturbances were generated using a displacement-type wavemaker, similar to that described by Walker (1973). In the quiescent state, the wavemaker paddle straddles the interface, as depicted in figure 1. Pulse-like disturbances are generated by imposing a single downward displacement of the paddle. This is accomplished by coupling the paddle to a geared drive motor through a scotch yoke. The drive motor, gear reduction unit, and the various moving parts are all mounted on structures attached directly to the floor of the laboratory. This assures that vibrations associated with operation of the wave-generating mechanism are decoupled from the tank itself.

The wavemaker has two degrees of freedom, *viz.* the length and duration of the paddle stroke, and these may be varied between 0–5 cm, and 0·5–5 seconds, respectively. It is important to recognize that the wavemaker does not have sufficient degrees of freedom to produce arbitrarily prescribed waveforms (e.g. solitary waves) as initial conditions to the experiment. It can only produce pulse-like disturbances which, in general, are not solitary waves. But, as previously noted, all of the evolution equations being studied in this investigation admit soliton solutions, so that the permanent waveform disturbances desired for the experiment were generated by adjusting the amplitude and duration of the paddle displacement (in an empirical fashion) such that a single soliton (plus a dispersive tail) emerged downstream of the wavemaker. Because the phase velocity of the soliton is greater than the group velocity of the tail, it separates from the oscillatory portion of the signal. Once the soliton has evolved and separated from the dispersive wavetrain, one is able to examine the important characteristics of this permanent waveform disturbance as it propagates through the test section. Following the aforementioned procedure, soliton disturbances in the amplitude range $0{\cdot}025 < \epsilon < 0{\cdot}5$ are readily generated in this facility.

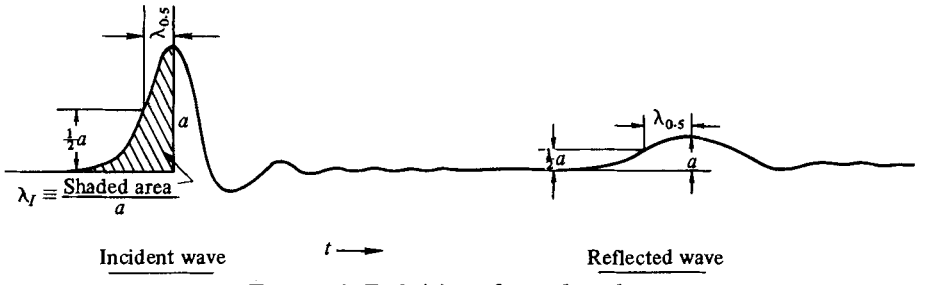

FIGURE 2. Definition of wavelength.

Measurement of the interfacial displacement were made using nine longitudinally displaced single-element capacitance gauges of the type described by Lake *et al.* (1977). These were mounted on five separate traversing mechanisms positioned above the water surface. The first probe was positioned 20 cm downstream of the wavemaker in order to record the initial disturbance created by the paddle displacement (see figure 1 for location and nomenclature of the remaining probes). The paddle displacement was monitored using a linear variable-displacement transducer (LVDT) mounted on the wavemaker. During the course of a run, the outputs of the nine capacitance gauges plus that of the LVDT were simultaneously recorded on a multichannel strip chart and on a 14-channel FM tape recorder.

Typically, experiments were initiated by starting the strip chart and tape recorder with the fluid in a quiescent state. The wavemaker was then actuated to yield a single downward thrust of the paddle. The resulting initial interfacial disturbance was recorded by the first probe, probe 1. Subsequently, this initial pulse-like wave evolved into a soliton followed by a dispersive wavetrain. These propagated down the tank past the eight data probes, probes $2a$–$5b$, reflected off the endwall, and propagated back through the test section in the opposite direction. When the reflected wave passed probe $2a$, the experiment was considered to be completed, and the monitoring equipment was shut off. Once the fluid had returned to a quiescent state (roughly 1–2 minutes later), the nine capacitance probes were calibrated by traversing them through the interface and correlating the probe output with its vertical position. The total elapsed time between the start of the experiment and the completion of the calibration was normally less than 5 minutes.

The above procedure was repeated several times using different values of the paddle displacement to generate various-amplitude waves. Following such a series of experiments, the FM analog tape was digitized at a rate of 100 samples/s per channel (real time), and the resulting digital data were stored for numerical processing. Typical quantities which were computed in the data-reduction program included the interfacial displacement (in engineering units) versus time for all nine capacitance gauges, and the maximum amplitude and horizontal extent of the incident and reflected waves recorded by each probe. Figure 2 illustrates the manner in which the amplitude and wavelength were computed. Note that only the forward portion of the soliton profile was used, since conditions in the 'wake' of the disturbance were never truly quiescent. Two definitions of the disturbance wavelength were used. The first, denoted $\lambda_{0.5}$, simply represents the half-amplitude point and is defined by

$$\frac{\eta(x-ct=\lambda_{0.5})}{a} = \frac{1}{2}.$$

A second definition, denoted λ_I, was also used and is given by

$$\lambda_I = \frac{1}{a}\int_0^\infty \eta(x-ct)\,d(x-ct).$$

Being an integral quantity, it is felt that λ_I provides a better (i.e. less noisy) measure of the soliton wavelength than does the half-amplitude point. This turns out to be an important consideration in analysing the results, since most of the data scatter is introduced through the experimental determination of the soliton wavelength. λ_I is related to the λ's used in the KdV, Benjamin–Ono, and finite-depth analyses (equations (3a), (5a) and (7a) respectively) as follows:

$$\begin{aligned} \text{KdV, } \lambda_I &= \lambda_{\text{KdV}}; \\ \text{Benjamin–Ono, } \lambda_I &= \tfrac{1}{2}\pi\lambda_{\text{B/O}}; \\ \text{Finite depth, } \lambda_I &= H\cot H/\lambda_{\text{FD}}. \end{aligned}$$

Two test conditions were chosen for consideration so that the depth effect upon the soliton amplitude–wavelength relationship could be investigated. These are identified as follows:

Configuration	$h = h_{\text{Freon}}$	$H = h_{\text{Freon}} + h_{\text{water}}$	H/h
Shallow water	1·366 cm	8·314 cm	6·086
Deep water	1·366 cm	49·236 cm	36·046

3.2. *Qualitative results and discussion of viscous effects*

The purpose of the present investigation is to study how the propagation characteristics of internal solitons are altered as one proceeds from a shallow-water system, presumably governed by the KdV equation, to a deep-water regime where the Benjamin–Ono analysis should be more appropriate. It has been previously emphasized that our primary concern is the study of permanent waveform disturbances. Of less importance for our purposes is what might be termed the period of evolution or generation; i.e. that period of time when an initial pulse-like disturbance (which is not a soliton) evolves into one or more solitons followed by a dispersive wavetrain. From an experimental point of view, it is important to ensure that this transient period of evolution is not long, relative to the time required for the disturbance to propagate to the end of the tank. Figure 3 presents the results of a preliminary test where the above criterion was not satisfied. The measurement was made using a Freon depth of about 7 cm, an overall fluid depth of about 40 cm. A single capacitance probe was positioned roughly 4 m from the wavenumber. Time increases to the right in this figure. The several pulses depicted in these records are a result of multiple reflections of the initial disturbance off the endwalls of the tank. The interesting feature to be observed in this figure is the extremely long evolution time required before a soliton is produced. Note, for example, that the initial pulse (which is not a soliton) propagates at least 36 m or roughly 6 tank lengths before one could say that the leading soliton is reasonably well separated from the remaining portion of the wavetrain. One also observes from this figure that the wavelength of the disturbance is quite long; being almost 50 % of the length of the tank.

Obviously, such features are undesirable from the standpoint of studying soliton characteristics, owing to the extremely long length of the disturbance (relative to the

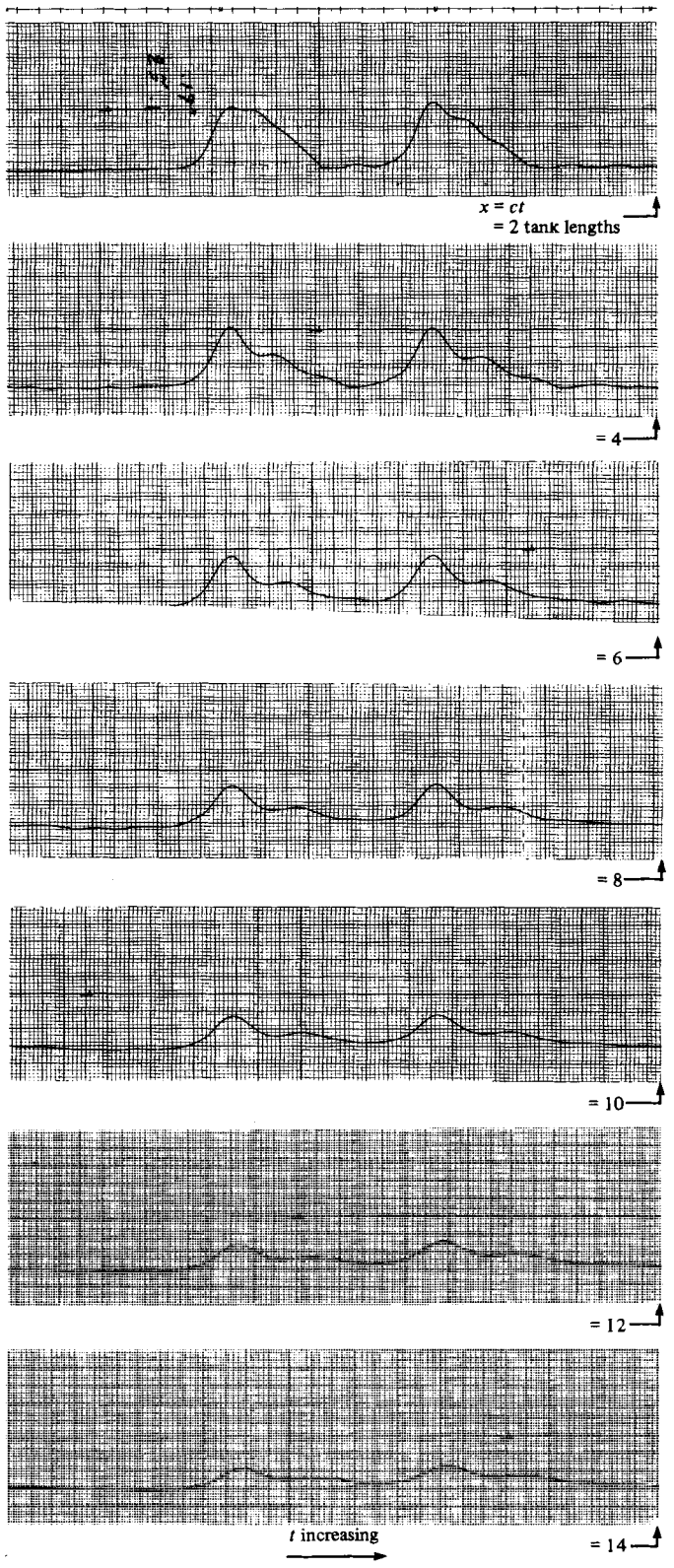

FIGURE 3. Results of a preliminary test; $h \simeq 7$ cm, $H \simeq 40$ cm.

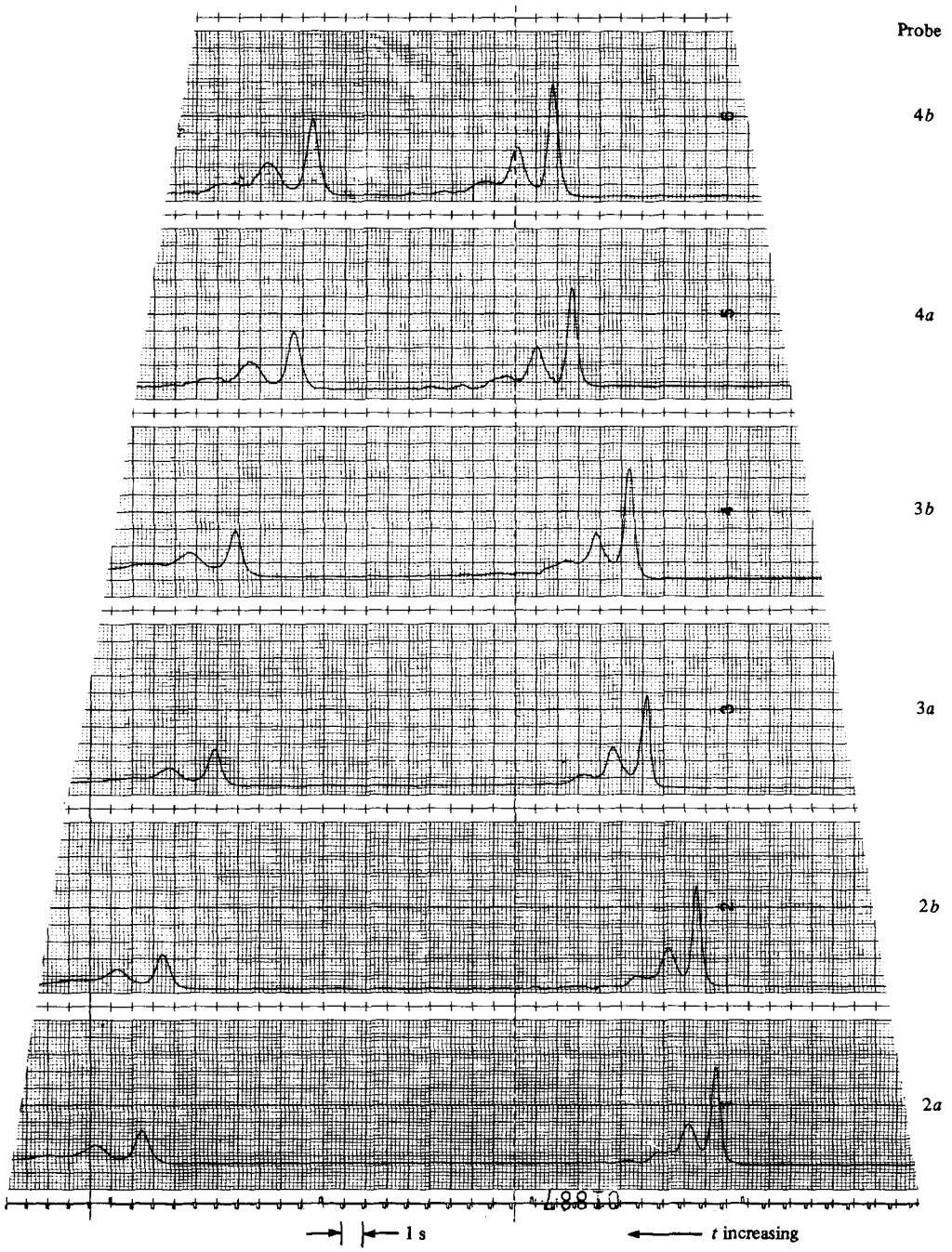

FIGURE 4. Example of multiple-soliton generation; shallow-water configuration.

length of the tank) and the predominance of endwall effects. These problems may be alleviated by sufficiently decreasing the fluid layer depths. Hammack & Segur (1974) present a simple argument for estimating the sorting time required for a soliton to separate from the dispersive portion of the wavetrain. Using their model (modified

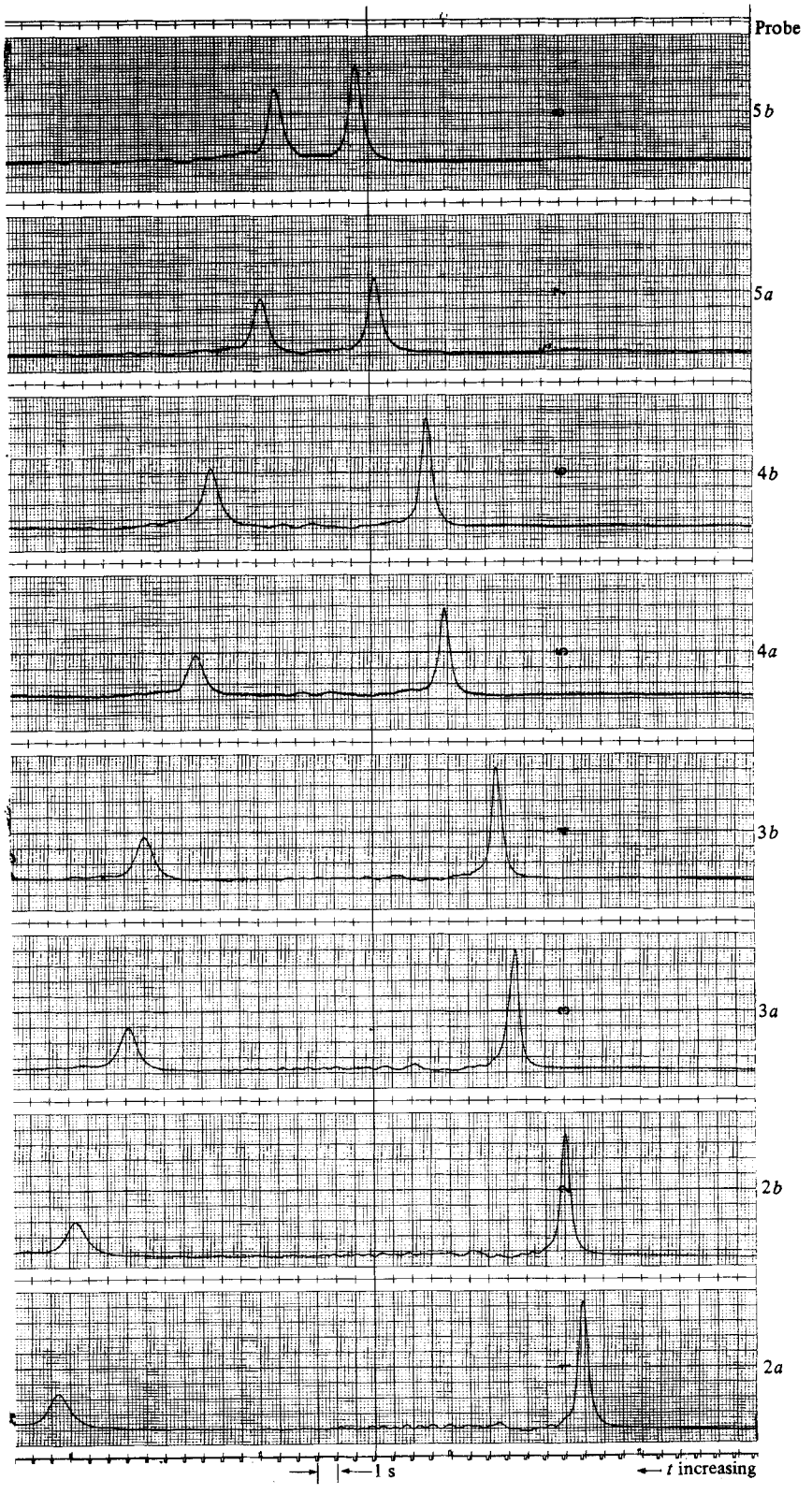

FIGURE 5. Example of single-soliton generation; shallow-water configuration.

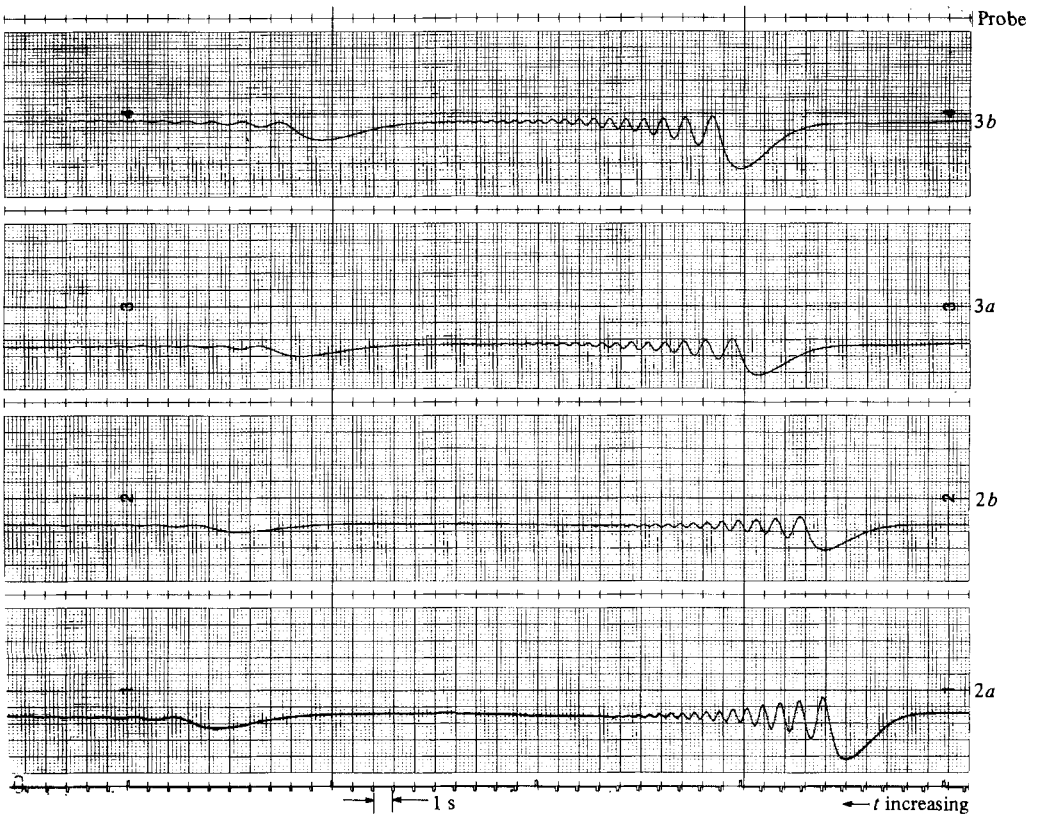

FIGURE 6. Example of the generation of a dispersive wavetrain; shallow-water configuration.

for an internal wave system), one estimates that, for a Freon layer depth of 1·5 cm, the sorting time for a typical wave in the present facility should be less than the time required for the pulse to propagate 50 per cent of the length of the tank. This is considered to be acceptable, and all of the remaining experiments were conducted using this nominal value for the depth of the Freon layer.

Having, in some sense, identified the best configuration for testing, several experiments were performed using the probe arrangement depicted in figure 1 to study qualitatively the evolution of the various types of disturbances which can be produced in this facility. Some typical results of these tests are presented in figures 4–6. The test conditions for these runs are those of the shallow-water configuration identified in § 3.1. Time increases to the left in these figures, and the second wave in each record is the reflection of the incident wave off the endwall of the tank. It should be pointed out that the sensitivities and gain settings of the various probes are not the same, so that relative-amplitude measurements between probes are not meaningful. Figure 4 presents a case where multiple solitons are formed from the initial condition. One observes here that at least two (and possibly three) solitons emerge. Note that, as the disturbance propagates down the tank, the relative spacings between adjacent peaks increases; a result of the difference in nonlinearity between the various solitons. Figure 5 shows the formation of a single soliton, followed by what appears to be a dispersive wavetrain. The data shown in this figure typify those which were used to obtain the quantitative results described in §§ 3.2 and 3.3.

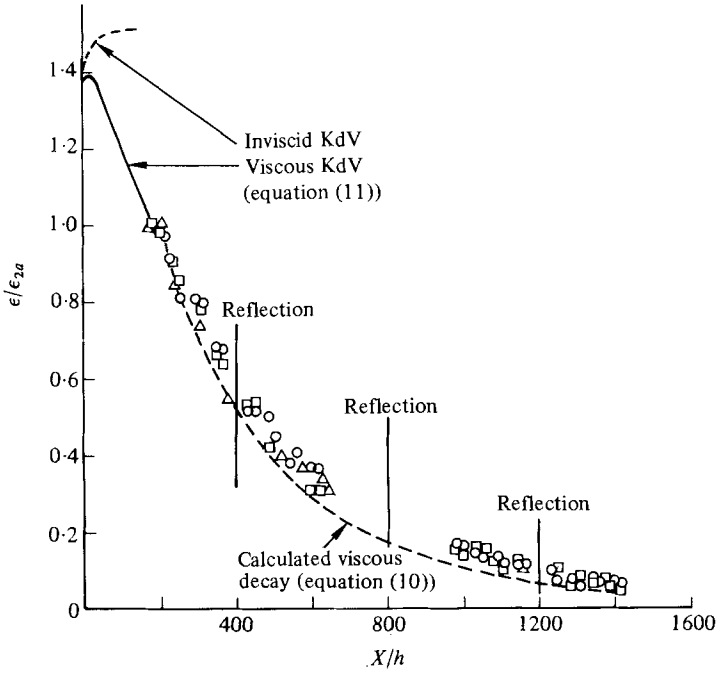

FIGURE 7. Viscous decay of interfacial wave amplitude. Initial conditions: measured profile for case C. ○, case A; □, case B; △, case C.

Finally, figure 6 shows a case where a dispersive wavetrain, but no soliton, is formed. The initial condition for this disturbance was a wave of depression, which was produced by reversing the direction of the wavemaker. That only an oscillatory waveform is generated from this initial condition is qualitatively consistent with the results of Hammack & Segur (1974) (their figure 7) and is predicted by the inverse-scattering solution of the KdV equation.

If we re-examine the single-soliton example shown in figure 5, it is found that, in actuality, a wave of permanent form is never realized experimentally. Note, for example, in the record for probe $2a$, that as a result of viscous dissipation the amplitude of the reflected wave is only about 30 per cent of the incident-wave amplitude. Clearly, viscosity has a non-negligible influence upon the propagation characteristics of the waves being studied in this investigation. To quantify the amount of such viscous attenuation, experiments were performed where multiple reflections off the endwalls were monitored in order to increase effectively the distance travelled by a given disturbance. The amplitude history of three such experiments (normalized by the incident-wave amplitude measured at probe $2a$) is shown in figure 7. Cases A and B represent data obtained in the deep-water configuration with initial amplitudes $\epsilon_{2a} = 0{\cdot}305$ and $0{\cdot}109$ respectively. Case C represents shallow-water data with $\epsilon_{2a} = 0{\cdot}269$. From these data, one sees that viscous dissipation acts to attenuate the wave amplitude by roughly 50 per cent per pass through the test section. These data are also useful as a basis for testing the viscous theories described in § 2.3. For example, figure 7 presents the numerically calculated solution to the viscous KdV equation (11), using as an initial condition the measured wave form recorded by probe 1 (20 cm from the wavemaker). Two calculations were performed, one with and one

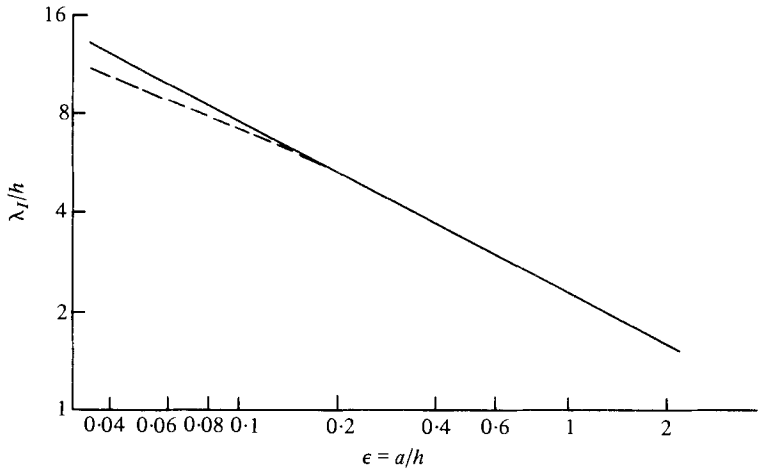

FIGURE 8. Effects of viscosity upon amplitude–wavelength scale relationship. ——, inviscid theory; – – –, viscous theory.

without the viscous term, and the output included the maximum disturbance amplitude as a function of propagation distance. From the results of the inviscid calculation, one finds that during the initial evolution period (when the leading soliton is being formed) the maximum amplitude grows. However, at about x/h equal to 80, the soliton has separated from the rest of the waveform, and beyond this point the maximum amplitude is constant. Examining the second calculation, one can clearly see the effect viscosity has upon the evolution of the initial disturbance. One finds, for example, that, for x/h less than about 10, the peak amplitude grows, but beyond this point viscosity becomes important, and the amplitude is attenuated by roughly 40 per cent before the solution merges into the data. Numerical difficulties prevented continuation of this calculation beyond about $x/h = 200$, but application of Keulegan's modified analysis, given by equation (10), yields reasonably good agreement with the remaining portion of the data.†

From this demonstration of the importance of viscosity on the disturbance amplitude, it is natural to ask how viscosity affects the soliton wavelength. This is an important question. Since the propagation characteristics of the interfacial waves are to be characterized in terms of their amplitude–wavelength relationship, it is necessary to establish whether this relationship has any functional dependence upon viscosity. In a qualitative sense, one may reason that, for a sufficiently large-amplitude soliton, the important dynamical balance lies between the nonlinear and dispersive terms in the governing equations. Viscosity should be important only in that it acts to attenuate the wave slowly, but should not directly influence the soliton scaling given by $a\lambda^2/h^3 = \text{constant}$ (this may be considered to be a quasi-steady approximation). It is clear, however, that, as viscosity acts to decrease the disturbance amplitude monotonically, eventually, the strengths of the viscous and nonlinear terms will become of comparable order. At this point, the quasi-steady approximation becomes invalid, and viscosity must enter directly into the scaling. The degree to which this scale relation is affected by viscosity is not easily predicted analytically,

† *Note added in proof*: use of the more-accurate expression of Hammack, Leone & Segur (1981) yields slightly better agreement with these data.

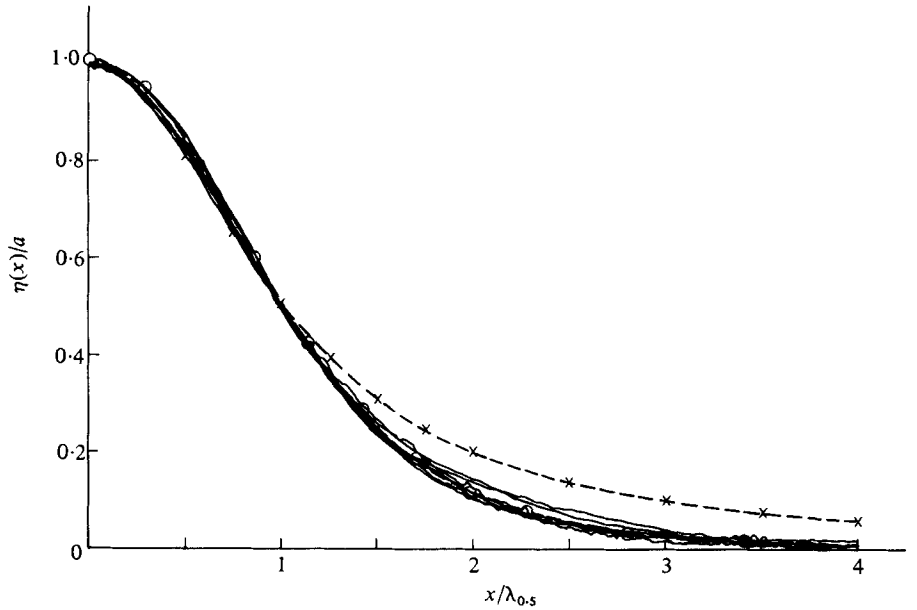

FIGURE 9. Profile shape $\eta(x)/a$ versus $x/\lambda_{0.5}$; shallow-water configuration. — —○— —, 'sech²'; — — × — — Lorentzian. Data compiled from runs: 4/25–1, $\epsilon = 0{\cdot}04$; 4/25–2, $\epsilon = 0{\cdot}05$; 4/25–1, $\epsilon = 0{\cdot}11$; 4/24–3, $\epsilon = 0{\cdot}18$; 4/25–6, $\epsilon = 0{\cdot}26$; 4/29–1, $\epsilon = 0{\cdot}57$; 4/29–1, $\epsilon = 0{\cdot}68$.

but we may again appeal to the numerical solutions of the viscous KdV equation and theoretically quantify what effects should be found in the present facility. The results of such a calculation are shown in figure 8 where $\lambda_I(t)/h$ is plotted versus $\epsilon(t)$ (with time appearing parametrically). For reference, the inviscid scaling $a\lambda_I^2/h^3 =$ constant is also presented. The initial condition for this calculation was a sech² profile (with $\epsilon(t = 0) = 0{\cdot}4$) having the proper solitary-wave amplitude–wavelength relationship as predicted by the inviscid theory. From these calculations, one finds that, for $\epsilon(t)$ greater than about 0·2, the amplitude–wavelength history follows the inviscid line, verifying the quasi-steady nature of the problem. As the amplitude decreases, however, viscosity begins to alter the scale relation in such a manner that λ_I/h grows more slowly than $\epsilon^{-\frac{1}{2}}$. The effect is not unduly large, though (except for very small waves, *viz.* $\epsilon < 0{\cdot}02$), and we conclude that viscous effects on the amplitude–wavelength scaling in the present facility are sufficiently small that meaningful measurements of this relationship may be obtained and compared with inviscid theoretical results.

3.3. *Quantitative results*

In the shallow-water configuration ($H/h = 6{\cdot}086$, $\Delta\rho/\rho = 0{\cdot}33$) twelve runs were made to examine the profile shape and amplitude–wavelength scale relationship for nonlinear internal solitons. Each run consisted of 16 realizations of a waveform (8 probes measuring incident and reflected waves), so that the shallow-water experiments yielded almost 200 profile measurements. In a strict sense, however, not all of these measurements may be considered to be totally independent, since any one run yields 16 measurements of the same disturbance, although one must remember that this wave is slowly varying in time due to viscosity, so that it is not *exactly* the same wave at each measurement station. The amplitudes of these waves varied over a

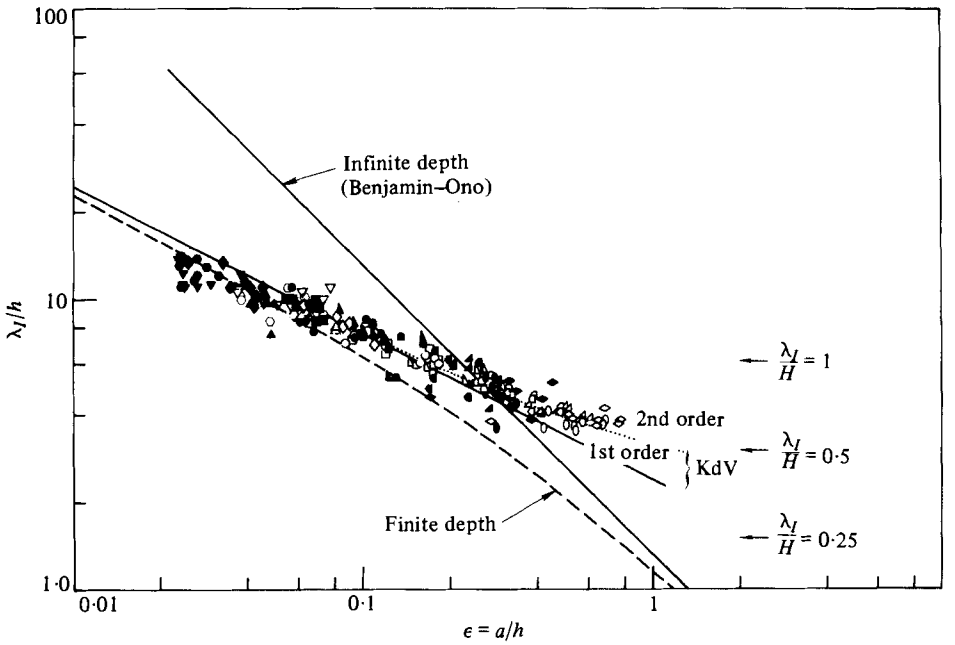

FIGURE 10. Amplitude–wavelength scale relationship; shallow-water configuration. (Solid symbols represent reflected waves.)

decade between $0{\cdot}025 < \epsilon < 0{\cdot}75$ with corresponding wavelength variations $4 < \lambda_I/h < 15$. Figure 9 presents the measured wave profile shape, $\eta(x)/a$ plotted versus $x/\lambda_{0{\cdot}5}$. In order to provide some estimate of the variance between profiles, seven individual wave-form realizations in the amplitude range $0{\cdot}04 < \epsilon < 0{\cdot}7$ are presented. For reference, both the 'sech^2' and Lorentzian profiles are also shown in this figure. Examination of the results reveals that the agreement between the shallow-water data and the 'sech^2' profile predicted by the KdV theory is quite good.

Such agreement between the theoretically predicted and experimentally measured wave forms is encouraging; but we have not subjected the theory to a very stringent test, because such profile comparisons introduce the artificial constraint of requiring the theory and experiment to agree at $x/\lambda_{0{\cdot}5} = 0$ and 1. For wave profiles that are reasonably similar, one would not expect large differences to occur between the two curves. A stronger test of the theory would be to establish whether the theoretically predicted one-parameter family of such 'sech^2' profiles or, in essence, the amplitude–wavelength relationship, is in agreement with the data. This is most conveniently displayed on a log–log scale, as shown in figure 10, where λ_I/h is plotted versus ϵ. These data represent amplitude–wavelength measurements of both the incident and reflected waves. As there may be some question regarding the validity of the reflected-wave data, since these waves are in effect seeing their own 'wake', these data are identified using solid symbols. In general one finds, though, that the incident and reflected wave data behave in a reasonably similar manner. Also shown in figure 10 are the theoretical scale relations predicted by the KdV, Benjamin–Ono and finite-depth analyses. Several comments may be made regarding the data shown in this figure. First of all, it is not unreasonable to expect that the Benjamin–Ono infinite-depth theory should poorly describe the results of a shallow-water experi-

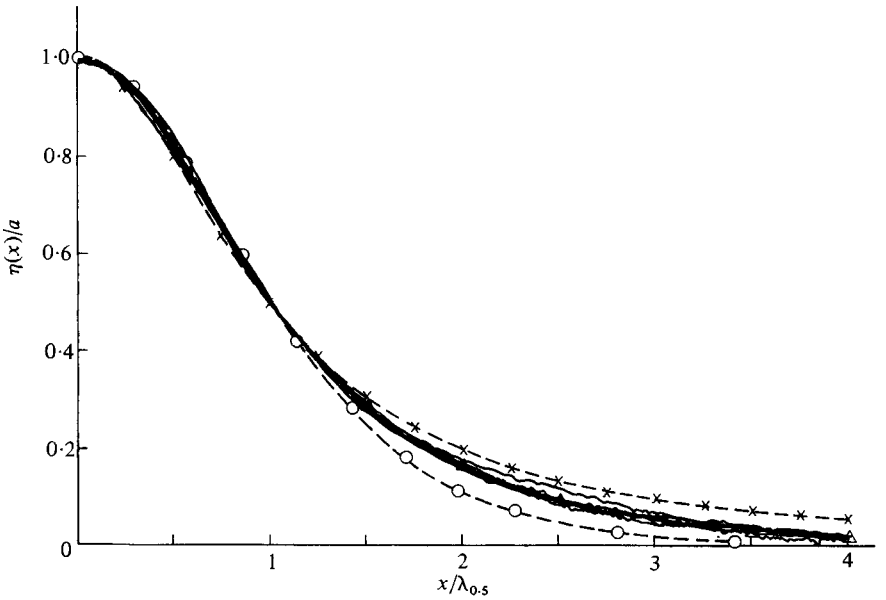

FIGURE 11. Profile shape $\eta(x)/a$ versus $x/\lambda_{0\cdot5}$; deep water configuration. — —○— —, 'sech²'; — —×— —, Lorentzian and finite depth ($\epsilon = 0{\cdot}06$); — —△— —, finite depth ($\epsilon = 0{\cdot}06$). Data compiled from runs: 4/27–3, $\epsilon = 0{\cdot}06$; 6/1–7, $\epsilon = 0{\cdot}08$; 6/1–4, $\epsilon = 0{\cdot}11$; 4/27–2, $\epsilon = 0{\cdot}11$; 6/1–1, $\epsilon = 0{\cdot}17$; 6/1–2, $\epsilon = 0{\cdot}26$; 6/1–2, $\epsilon = 0{\cdot}56$.

ment. Indeed, this is observed in figure 10 where one finds that the slope of the Benjamin–Ono line is in total disagreement with the data. The finite-depth theory does better, but the shallow-water KdV theory yields by far the best agreement with the data. The agreement, though, is by no means exact. One notes, for example, that for ϵ less than about 0·05 the theory slightly overpredicts the experimentally measured wavelengths by 10–15 per cent. This is not inconsistent with our previous discussion (§3.2) regarding the effects of viscosity on the amplitude–wavelength scale relationship. There it is shown that numerical solutions of the viscous KdV equation (11) yield wavelengths which are somewhat smaller than those the inviscid theory would predict for values of ϵ less than about 0·1. One suspects, then, that, for the very-small-amplitude portion of the data, the nonlinear effects have been weakened to such an extent that the viscous terms are of comparable order. This argument seems plausible, but could be significantly strengthened by additional experimentation. Over the remaining portion of the data the slope of the KdV theory and the data are reasonably close, but for ϵ greater than about 0·2 the theory slightly underpredicts the measurements. However, the second-order KdV theory, derived in §2.2, shows noticeably better agreement with the data, indicating that the small discrepancy between the data and the first-order theory for $\epsilon > 0{\cdot}2$ is likely due to higher-order nonlinear effects.

Upon completion of the shallow-water experiments, the overall fluid depth ratio was increased to $H/h = 36{\cdot}044$ and eight additional experiments were conducted to ascertain what effect the increased depth has upon the amplitude–wavelength scale relationship. The range of amplitudes studied varied between $0{\cdot}03 < \epsilon < 0{\cdot}6$ with a corresponding span of wavelengths $4 < \lambda_I/h < 20$. Note that' in terms of the total

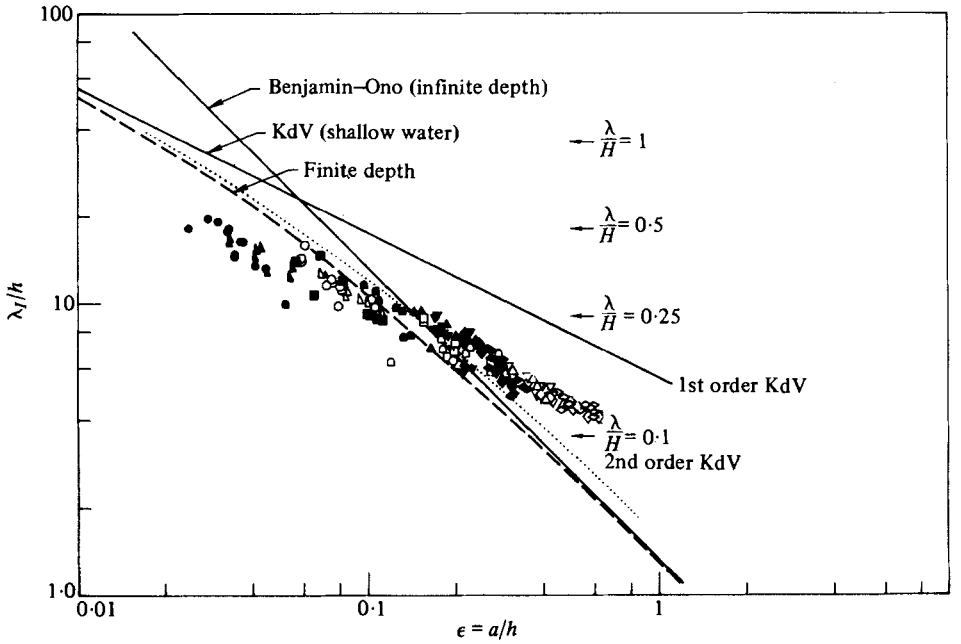

FIGURE 12. Amplitude–wavelength scale relationship; deep-water configuration. (Solid symbols represent reflected waves.)

fluid depth H, $0{\cdot}11 < \lambda_I/H < 0{\cdot}56$. Hence, for these experiments the depth is always greater (and in some cases much greater) than the wavelength of the disturbance.

Figure 11 presents the measured deep-water profile shape, $\eta/\lambda_{0{\cdot}5}$. Again, to provide some degree of statistical significance seven individual wave records in the amplitude range $0{\cdot}06 < \epsilon < 0{\cdot}6$ are presented. For reference both the 'sech^2' and Lorentzian profile shapes are shown. In addition, wave profiles corresponding to Joseph's (1977) solitary-wave solution to the finite-depth equation are also presented. The two finite-depth profiles depicted are for $\epsilon = 0{\cdot}06$ and $\epsilon = 0{\cdot}6$; i.e. the range of ϵ over which the data were compiled (note that the $\epsilon = 0{\cdot}6$ finite-depth profile is indistinguishable from the infinite-depth Lorentzian profile). We note from this figure that most of the data lie between the 'sech^2' and Lorentzian profiles particularly in the tails of the waves. The $\epsilon = 0{\cdot}06$ finite-depth theory ostensibly yields good agreement with the data, but actually all the data should lie between the two curves $\epsilon = 0{\cdot}06$ and $\epsilon = 0{\cdot}6$, rather than being centred on the $\epsilon = 0{\cdot}06$ profile. Thus, one must conclude that even this relatively weak comparison between the theory and the data, involving the normalized profile shape, does not yield a conclusive result.

Figure 12 presents the amplitude–wavelength scaling measured for the deep-water runs, together with the theoretical scaling predicted by the KdV, Benjamin–Ono, and finite-depth analyses. Again, one sees that none of the three theories accurately (or even approximately) describes the experimental results. The extent to which all of these theories are in disagreement with the data is, perhaps, somewhat surprising, particularly in light of the reasonably good results obtained in the shallow-water experiments. For example, one notes that the KdV theory has a slope which agrees fairly well with the data (on a log–log plot), but overpredicts λ_I/h by a factor of almost 2. The second-order KdV theory exhibits much the same

behaviour that was observed in the shallow-water configuration, but does not lead to any improvement in agreement with the data. For the Benjamin–Ono and finite-depth analysis, one finds that both theories intersect the data, but clearly have the wrong slope.

4. Discussion of results and conclusions

Based upon the experimental results discussed in the previous section, the following general observations may be made. First, in the shallow-water configuration the first-order inviscid Korteweg–de Vries theory agrees in a reasonably quantitative manner with the experimental data with regards to the profile shape and the soliton amplitude–wavelength relationship. In particular, one finds that the profile shape matches the predicted 'sech^2' profile almost exactly. Furthermore, the amplitude–wavelength relationship predicted by the first-order theory is valid for wave amplitudes as large as $\epsilon \approx 0{\cdot}2$, and the inclusion of second-order nonlinear terms extends the useful range of the KdV theory to wave amplitudes of $\epsilon \approx 0{\cdot}8$. The viscous effects discussed in §3.2 appear to slightly alter the amplitude–wavelength relationship for small amplitudes, roughly $\epsilon < 0{\cdot}1$, but these deviations from the inviscid theory are not large, and presumably could be accounted for using the viscous KdV equation given by equation (11). In short, one concludes that the present investigation has quantitatively validated the adequacy of the Korteweg–de Vries analysis as applied to internal waves in fluids of limited vertical extent.

Having noted the reasonably good results of the first portion of the investigation, the obvious question which arises is why the experimental results of the deep-water experiments are described so poorly by any of the available theories. Since the identical procedures and data-processing techniques were used on both the deep- and the shallow-water data, we feel that the deep-water experimental results are not in error. With regard to the theoretical analyses, the following comments may be made. All of the theories discussed in this paper consider fluid systems having wave motions which are both weakly nonlinear and in some sense long. In the Korteweg–de Vries analysis, 'long' is measured relative to the total depth of the fluid. In the deep-water configuration, using the theoretical KdV scale relationship, the wavelength λ is predicted to be 'long' relative to the total depth H (say, $\lambda/H \geqslant 10$) when ϵ is smaller than about 0·001. Hence, in the deep-water configuration the radius of convergence of the KdV theory is extremely limited. Since most of the data lie in the amplitude range $0{\cdot}025 < \epsilon < 0{\cdot}6$, the disagreement between the theory and experiment is not unexpected.

A similar argument may be made regarding the Benjamin–Ono analysis. Here, the assumption is made that the wavelength is much shorter than the overall fluid depth. In the deep-water configuration, this theory would predict that λ is much smaller than H (say $\lambda/H < 0{\cdot}1$) when ϵ is greater than about 0·5. However, in this region the weak nonlinearity assumption is violated, and one again concludes that the disagreement with the data probably results from the theory being applied outside of its domain of validity.

The failure of the finite-depth theory to describe the data adequately is a more difficult matter to explain. Ostensibly, the important assumptions which are inherent in this theory are that the waves are weakly nonlinear, and that the thermocline is

thin relative to the total fluid depth. No constraint is placed upon the wavelength of the disturbance, other than it must be long relative to the thermocline thickness. Consider first the weak nonlinearity assumption. If one may extrapolate from the results of the shallow-water experiments, one would conclude that this assumption is justified for waves having amplitudes smaller than about $\epsilon = 0{\cdot}2$. At least a portion of the deep-water data lie in this parameter range, but even here there is total disagreement between the theory and the experiment.

Regarding the second assumption dealing with the thinness of the thermocline, one might question whether a depth ratio $H/h = 36{\cdot}044$ is sufficiently large to be classified as a 'thin' thermocline. This question may be resolved in the following manner. In the finite-depth theory, the thin-thermocline assumption is made in order to simplify the dispersion relation (for arbitrary stratification) to an analytic form. In the two-layer system, however, the dispersion relation is already known in exact analytic form (cf. Lamb 1932, p. 371). Hence, if one is willing to accept numerical solutions, one could substitute this exact analytic representation into the dispersive term of Whitham's equation, and check to see if the computed results are significantly different from those predicted by the finite-depth theory. These calculations were performed, using the pseudo-spectral code previously mentioned, with depth and density ratios corresponding to those of the deep-water configuration, and wave amplitudes ranging between $0{\cdot}01 < \epsilon < 1$. For a given value of ϵ, the initial condition to the program was the wave profile predicted by Joseph's (1977) solitary-wave solution to the finite-depth equation, and the calculations were run for times between $t = 0$ and $t = 20$ seconds, which roughly corresponds to the time required for a pulse to make two transits through the test section of the channel. If the thin-thermocline assumption is a valid approximation in the present deep-water configuration, then Joseph's profile should also be the solitary wave solution of the more general equation. This, in fact, turns out to be the case. The calculations revealed that use of the exact dispersion relation had almost negligible influence on Joseph's profile, causing a modest change in the wave amplitude of typically about 1 % during the computation time. On the basis of these calculations, then, one must conclude that the disagreement between the finite-depth theory and the experimental data is not a result of applying the theory outside of its domain of validity.

At this time, the present authors do not see a way of resolving this apparent discrepancy between our data and the existing theoretical analyses. We note, however, that similar results have recently been reported by Hammack, Leone & Segur (1981). In this work, the experimentally measured soliton half-amplitude wavelength ($\epsilon = 0{\cdot}18$, $H/h = 9$) is underpredicted by the finite-depth theory by about 20 %, quite consistent with our results. Clearly, further work in this area is required before a conclusive statement may be made regarding the proper theory to be used in physical systems where the disturbance wavelength is comparable to the total fluid depth.

The authors gratefully acknowledge several valuable discussions with Dr B. M. Lake and Dr C. Hindman. We are also indebted to Dr H. Segur for comments made regarding our viscous theory. Finally, they would like to thank Mr D. J. Rowland for his help in constructing the experimental facility. This study was sponsored by The Johns Hopkins University/Applied Physics Laboratory, under Contract no. 600613.

Appendix A. Extension of the KdV equation to second order

Consider a two-fluid system bounded above and below by rigid walls. The lower- and upper-layer densities are ρ_1 and ρ_2, and the corresponding fluid depths are h_1 and h_2. The relevant equations and boundary conditions are given by

$$\left.\begin{aligned} \nabla^2\phi_{1,2} = 0, \quad \phi_{1_z}(z=h_1) = \phi_{2_z}(z=h_2) = 0, \\ \eta_t + \phi_{1_x}\eta_x - \phi_{1_z} = 0, \\ \eta_t + \phi_{2_x}\eta_x - \phi_{2_z} = 0, \\ [\![\{\rho\phi_t + \tfrac{1}{2}(\nabla\phi)^2 + g\eta\}]\!] = 0, \end{aligned}\right\} z = \eta(x,t). \tag{A 1}$$

Introducing the slow space and time scales

$$\xi = \epsilon^{\frac{1}{2}}(x - c_0 t), \quad \tau = \epsilon^{\frac{3}{2}}t,$$

where $\epsilon = a/(h_1+h_2)$, and expanding the velocity potential and interfacial displacement as

$$\phi = \epsilon^{\frac{1}{2}}[\phi_{(1)}(\xi,\tau,z) + \epsilon\phi_{(2)}(\xi,\tau,z) + \ldots],$$

$$\eta = \epsilon\eta_{(1)}(\xi,\tau) + \epsilon^2\eta_{(2)}(\xi,\tau) + \ldots,$$

and solving (A 1) recursively, one finds c_0^2 at $O(\epsilon)$,

$$\eta_{(1)_\tau} + c_1\eta_{(1)}\eta_{(1)\xi} + c_2\eta_{(1)\xi\xi\xi} = 0 \tag{A 2}$$

at $O(\epsilon^2)$, and

$$\eta_{(2)_\tau} + c_1[\eta_{(1)}\eta_{(2)}]_\xi + c_2\eta_{(2)\xi\xi\xi} + c_3\eta_{(1)\xi} + c_4[\eta_{(1)}\eta_{(1)\xi\xi}]_\xi + c_5[\eta_{(1)}^3]_\xi + c_6[\eta_{(1)\xi}^2]_\xi = 0 \tag{A 3}$$

at $O(\epsilon^3)$. Combining (A 2) and (A 3), we obtain the KdV equation extended to $O(\epsilon^2)$ written as

$$\eta_t + c_0\eta_x + c_1\eta\eta_x + c_2\eta_{3x} + c_3\eta_{5x} + c_4(\eta\eta_{xx})_x + c_5(\eta^3)_x + c_6(\eta_x^2)_x = 0, \tag{A 4}$$

where

$$\begin{aligned} c_0^2 &= g(\rho_1-\rho_2)h_2h_1/(\rho_2h_1+\rho_1h_2), \\ c_1 &= (c_0/h_1)\times 3(1-s/r^2)/2(1+s/r) = (c_0/h_1)\tilde{c}_1, \\ c_2 &= (c_0h_1^2)r(s+1/r)/6(1+s/r) = (c_0h_1^2)\tilde{c}_2, \\ c_3 &= (c_0h_1^4)[r^3(s+1/r^3)/90(1+s/r) + 3\tilde{c}_2^2/2] = (c_0h_1^4)\tilde{c}_3, \\ c_4 &= (c_0h_1)[(s-1)/6(1+s/r) + 7\tilde{c}_1\tilde{c}_2/3] = (c_0h_1)\tilde{c}_4, \\ c_5 &= (c_0/h_1^2)[-(1+s/r^3)/(1+s/r) + 7\tilde{c}_1^2/18)] = (c_0/h_1^2)\tilde{c}_5, \\ c_6 &= (c_0h_1)[(s-1)/12(1+s/r) + 17\tilde{c}_1\tilde{c}_2/12)] = (c_0h_1)\tilde{c}_6, \\ s &= \rho_2/\rho_1, \quad r = h_2/h_1. \end{aligned}$$

The amplitude–wavelength scale relationship is given to second order by

$$\left(\frac{h}{\lambda}\right)^2 = \alpha^{(1)}\frac{a}{h} + \alpha^{(2)}\left(\frac{a}{h}\right)^2, \tag{A 5}$$

where

$$\begin{aligned} \alpha^{(1)} &= \tilde{c}_1/12\tilde{c}_2, \\ \alpha^{(2)} &= -\tilde{c}_4\alpha^{(1)}/12\tilde{c}_2 - 5\alpha^{(1)^2}\tilde{c}_3/\tilde{c}_2 + \tilde{c}_6\alpha^{(1)}/6\tilde{c}_2 + \tilde{c}_5/8\tilde{c}_2. \end{aligned}$$

The constant C in (9a) is defined by

$$C = 3\tilde{c}_4/4\tilde{c}_2 - 15\tilde{c}_3\alpha^{(1)}/\tilde{c}_2 - \tilde{c}_5/8\tilde{c}_2\alpha^{(1)} + \tilde{c}_6/2\tilde{c}_2. \tag{A 6}$$

The preceding analysis assumes the upper boundary condition to be a rigid lid. An analysis assuming a free-surface condition proceeds along similar lines, and the resulting amplitude–wavelength scale relationship is given by

$$\frac{a}{h_1} = \tfrac{4}{3}r^2\frac{1+rs[1-(1-\sigma)^3]/\sigma}{r^2-\sigma^3 s}\left(\frac{h_1}{\lambda}\right)^2 \Bigg/ \left\{1-\tfrac{4}{3}r^2\frac{1+rs[1-(1-\sigma^3)]/\sigma}{r^2+rs\sigma^2}\left(\frac{h_1}{\lambda}\right)^2\right\}, \tag{A 7}$$

where

$$\sigma = \frac{r}{s}(1-s)\left[\frac{1+r}{2} - \left\{\left(\frac{1+r}{2}\right)^2 - r(1-s)\right\}^{\frac{1}{2}}\right]^{-1} - \frac{r}{s}. \tag{A 8}$$

Appendix B. Viscous damping of internal solitary waves

Consider a two-fluid system confined between two rigid walls where the interfacial displacement η is a solitary wave given by

$$\eta(x,t) = a\,\mathrm{sech}^2\left(\frac{x-ct}{\lambda}\right),$$

where

$$\frac{a\lambda^2}{h_1^3} = \alpha(\rho_1, \rho_2, h_1, h_2)$$

and ρ_1, ρ_2, h_1, h_2 are the lower- and upper-layer densities and fluid depths, respectively.

Following Keulegan (1948), the wave-induced fluid velocity in the wall boundary layer for the lower layer is given by

$$u_1(x,z,t) = \frac{ac}{h_1}\left[\mathrm{sech}^2\left(\frac{x-ct}{\lambda}\right) - \frac{2}{\pi^{\frac{1}{2}}}\int_0^\infty \mathrm{sech}^2\left(\frac{x-ct}{\lambda} + \frac{cz^2}{4\lambda\nu_1\beta^2}\right)e^{-\beta^2}\,d\beta\right],$$

where ν_1 is the lower-layer kinematic viscosity. A similar expression may be written for the upper-boundary-layer flow. The rate of energy dissipation, dE_v/dt, in the lower boundary layer is given by (Keulegan 1948)

$$\frac{dE_v}{dt} = \rho_1\nu_1 B\int_{-\infty}^{\infty}\frac{ac}{h_1}\mathrm{sech}^2\left(\frac{x-ct}{\lambda}\right)\left.\frac{\partial u_1}{\partial z}\right|_{z=0} d(x-ct),$$

where B is the breadth of the channel. The total energy dissipated in the lower layer includes contributions from the channel side walls and the sheared interfacial region. The side-wall contribution may be calculated through geometrical parameters. The interfacial contribution could be calculated by examining the boundary-layer flow in this region, but, for simplicity, we assume that the contribution from the interfacial shear region (in the lower layer) is simply equal to that due to the lower-wall boundary layer. Although approximate, we feel that this is not too unreasonable, and the analysis is somewhat simplified.† Dissipation in the upper layer is computed in a similar manner, except that the contribution from the upper-wall boundary layer is neglected. This is because the upper boundary in the experiment is a free surface and should behave as a stress-free boundary.

† *Note added in proof*: Hammack *et al.* (1981) perform the analysis within the interfacial region.

The total energy contained in the wave field, E_T, is given by

$$E_T = \tfrac{4}{3}Bg\Delta\rho h_1^3 \alpha^{\frac{1}{2}}\epsilon^{\frac{3}{2}},$$

where $\epsilon = a/h_1$ and $\Delta\rho = \rho_2 - \rho_1$. Assuming $\alpha \neq \alpha(t)$ (i.e. a quasi-steady assumption), we may differentiate this expression with respect to time, and equate this with the total rate of energy dissipation. After some manipulation, one gets an expression for the amplitude decay of the solitary wave, given by

$$\frac{\epsilon(x)}{\epsilon_0} = \left[1 + \epsilon_0^{\frac{1}{4}} K \frac{x - x_0}{h_1}\right]^{-4},$$

where

$$K = \frac{1}{2\pi^{\frac{3}{2}}} \frac{c^{\frac{3}{2}}\nu_1^{\frac{1}{2}}\rho_1}{g\Delta\rho h_1^{\frac{3}{2}}\alpha^{\frac{1}{4}}} \left[2\left(1 + \frac{h_1}{B}\right) + \left(\frac{h_1}{h_2}\right)^2 \frac{\rho_2}{\rho_1}\left(\frac{\nu_2}{\nu_1}\right)^{\frac{1}{2}}\left(1 + \frac{2h_2}{B}\right)\right].$$

In the limit $\rho_2 \to 0$, the above expression reduces to that derived by Keulegan (one needs to exclude the contribution from the interfacial region) for the slow viscous damping of a surface solitary wave.†

Appendix C. Evolution equation for long internal waves in a viscous medium

The following analysis closely follows that of Kakutani & Matsuuchi (1975). Consider a fluid system with a mean density profile $\bar{\rho}(z)$ which is confined between an upper and lower boundary, separated by a distance H; ρ_0 is a reference density, g is the acceleration due to gravity, and the vertical co-ordinate z is zero at the lower boundary. The flow field is divided into two inner regions, lying in the neighbourhood of the viscous boundary layers on the rigid surfaces, and an outer region sufficiently far removed from the boundaries that viscous effects are negligible.

Introducing the KdV scaling

$$\xi = \epsilon^{\frac{1}{2}}(x - c_0 t), \quad \tau = \epsilon^{\frac{3}{2}}t,$$

where ϵ measures the wave displacement and c_0 is the linear long-wave phase speed, expanding the outer dependent variables (denoted $u^{(0)}$, $w^{(0)}$, ...) as

$$u^{(0)} = \epsilon u_1^{(0)} + \epsilon^2 u_2^{(0)} + \ldots,$$
$$w^{(0)} = \epsilon W^{(0)} = \epsilon[\epsilon w_1^{(0)} + \epsilon^2 w_2^{(0)} + \ldots],$$

and requiring the $O(\epsilon^2)$ system of equations to have non-singular solutions yields

$$\left[-\int_0^H \frac{2}{c_0}\phi(\bar{\rho}\phi')'\,dz\right] f_\tau + \left[\int_0^H \phi J(\bar{\rho}, \phi)\,dz\right] f f_\xi + \left[\int_0^H \bar{\rho}\phi^2\,dz\right] f_{\xi\xi\xi}$$
$$= \bar{\rho}[\phi w_2^{(0)\prime} - \phi' w_2^{(0)}]|_{z=0}^{H}. \quad \text{(C 1)}$$

Here, primes denote differentiation with respect to z, the stream function $\psi = f(\xi, \tau)\phi(z)$, and $J(\bar{\rho}, \phi)$ is given by

$$J(\bar{\rho}, \phi) = \frac{1}{c_0}\left[\left\{-\bar{\rho}(\phi')^2 + \bar{\rho}\phi\phi'' - \frac{c_0^2}{g}\phi'(\bar{\rho}\phi')'\right\}' - \phi'(\bar{\rho}\phi')' + \phi(\bar{\rho}\phi')''\right].$$

† Note that Keulegan approximates $12^{\frac{1}{4}}/4\pi^{\frac{3}{2}}$ as $\frac{1}{12}$.

The velocity potential ϕ is determined through the eigenvalue problem (with as yet unspecified boundary conditions)

$$(\bar{\rho}\phi')' - \frac{gH}{c_0^2}\bar{\rho}'\phi = 0.$$

In order to proceed, one needs to consider the inner viscous problem so that boundary conditions on ϕ, $w_2^{(0)}$, and $w_2^{(0)\prime}$ may be prescribed at $z = 0, H$.

Within the viscous inner regions, the characteristic vertical length scale is the boundary-layer thickness, which for the present experiment can be shown to be $O(\epsilon)$. Thus, the appropriate inner variables are defined as

$$\eta_1 = z/\epsilon, \quad \eta_2 = (H-z)/\epsilon,$$

where η_1 and η_2 are the stretched co-ordinates in the lower and upper boundary layers, respectively. ξ and τ remain as previously defined. Substituting this scaling into the governing equations, expanding the inner dependent variables in powers of ϵ, and matching with the outer flow solution yields

$$\begin{aligned} \phi(0) &= 0, \\ w_2^{(0)}(0) &= \left(\frac{g}{H}\right)^{\frac{1}{4}} \frac{1}{(\pi R_1^* c_0)^{\frac{1}{2}}} \int_\xi^\infty \frac{\partial f}{\partial \xi'} \frac{d\xi'}{(\xi'-\xi)^{\frac{1}{2}}}, \\ w_2^{(0)\prime}(0) &= 0, \end{aligned} \tag{C 2}$$

where $R_1^* = (gH^{\frac{1}{2}}H/\nu_1)\epsilon^{\frac{5}{2}}$, and ν_1 is the kinematic viscosity at the lower boundary. A similar expression may be derived for the upper boundary layer.

Substituting (C 2) into (C 1) yields the long-wave evolution equation

$$f_\tau + c_1 f f_\xi + c_2 f_{\xi\xi\xi} = c_3 \int_\xi^\infty \frac{\partial f}{\partial \xi'} \frac{d\xi'}{(\xi'-\xi)^{\frac{1}{2}}}, \tag{C 3}$$

where

$$c_1 = \frac{3}{2}\frac{\int_0^H \bar{\rho}(\phi')^3\,dz}{\int_0^H \bar{\rho}(\phi')^2\,dz}, \quad c_2 = \frac{c_0}{2}\frac{\int_0^H \bar{\rho}\phi^2\,dz}{\int_0^H \bar{\rho}(\phi')^2\,dz},$$

$$c_3 = \frac{H}{2}\left(\frac{g}{H}\right)^{\frac{1}{4}}\left(\frac{c_0}{\pi}\right)^{\frac{1}{2}}\left[\frac{\bar{\rho}(H)\phi'^2(H)}{R_2^{*\frac{1}{2}}} + \frac{\bar{\rho}(0)\phi'^2(0)}{R_1^{*\frac{1}{2}}}\right] \Big/ \int_0^H \bar{\rho}(\phi')^2\,dz$$

and c_0 and ϕ are determined through the eigenvalue problem

$$(\bar{\rho}\phi')' - \frac{gH}{c_0^2}\bar{\rho}'\phi = 0, \quad \phi(0) = \phi(H) = 0.$$

We note here that this model was formulated under the assumption that $\bar{\rho}(z)$ is a continuous function. Hence the boundary layer within the interfacial shear region of the present experiment has not been explicitly included. For the purposes of making comparisons with the experimental data, we included the interfacial shear effects (as well as side-wall effects) in an *ad hoc* fashion by making appropriate modifications to the coefficient c_3 in (C 3), consistent with what was done in appendix B.

REFERENCES

BENJAMIN, T. B. 1966 Internal waves of finite amplitude and permanent form. *J. Fluid Mech.* **25**, 241.

BENJAMIN, T. B. 1967 Internal waves of permanent form in fluids of great depth. *J. Fluid Mech.* **25**, 559.

BENNEY, C. J. 1966 Long nonlinear waves in fluid flows. *J. Math. Phys.* **45**, 52.

CHEN, H. H., LEE, Y. C. & PEREIRA, N. R. 1979 Algebraic internal wave solitons and the integrable Calogero–Moser–Sutherland N-body problem. *Phys. Fluids* **22**, 187.

CHRISTIE, D. R., MUIRHEAD, K. & HALES, A. 1978 On solitary waves in the atmosphere. *J. Atm. Sci.* **35**, 805.

DAVIS, R. E. & ACRIVOS, A. 1967 Solitary internal waves in deep water. *J. Fluid Mech.* **29**, 593.

FORNBERG, B. E. 1977 On a Fourier method for the integration of hyperbolic equations. *SIAM J. Numerical Analysis* **12**, 509.

HAMMACK, J., LEONE, C. & SEGUR, H. 1981 Long internal waves. (To be published.)

HAMMACK, J. L. & SEGUR, H. 1974 The Korteweg–de Vries equation and water waves. Part 2. Comparison and experiments. *J. Fluid Mech.* **65**, 289.

JOSEPH, R. I. 1977 Solitary waves in a finite depth fluid. *J. Phys.* A, *Math. General* **10**, L225.

KAO, T. & PAO, H. P. 1979 Wake collapse in the thermocline and internal solitary waves. *J. Fluid Mech.* **97**, 115.

KAKUTANI, T. & MATSUUCHI, K. 1975 Effect of viscosity on long gravity waves. *J. Phys. Soc. Japan* **39**, 237.

KEULEGAN, G. H. 1948 Gradual damping of solitary waves. *N.B.S. J.* **40**, 480.

KUBOTA, T., KO, D. R. S. & DOBBS, L. D. 1978 Propagation of weakly nonlinear internal waves in a stratified fluid of finite depth. *A.I.A.A. J. Hydronautics* **12**, 157.

LAKE, B. M., YUEN, H. C., RUNGALDIER, H. & FERGUSON, W. 1977 Nonlinear deep-water waves: theory and experiment. Part 2. Evolution of a continuous wave train. *J. Fluid Mech.* **83**, 49.

LAMB, H. 1932 *Hydrodynamics*, 6th edn. Cambridge University Press.

MATSUUCHI, K. 1976 Numerical investigations on long gravity waves under the influence of viscosity. *J. Phys. Soc. Japan* **41**, 681.

MEISS, J. D. & PEREIRA, N. R. 1978 Internal wave solitons. *Phys. Fluids* **21**, 700.

ONO, H. 1975 Algebraic solitary waves in stratified fluids. *J. Phys. Soc. Japan* **39**, 1082.

OSBORNE, A., BURCH, T. & SCARLET, R. 1978 The influence of internal waves on deep water drilling. *J. Petroleum Tech.* 1497.

OSBORNE, A. & BURCH, T. 1980 Internal solitons in the Andaman Sea. *Science* (submitted).

SEGUR, H. 1973 The Korteweg–de Vries equation and water waves. Solutions of the equations. Part 1. *J. Fluid Mech.* **59**, 721.

WALKER, L. R. 1973 Interfacial solitary waves in a two fluid medium. *Phys. Fluids* **16**, 1796.

YATES, C. 1978 An experimental study of internal solitary waves. *AIAA 16th Aerospace Sciences Meeting, Huntsville, Alabama*, Paper no. 78–262.